Highly Realistic Visual Simulation of Outdoor Scenes Under Various Atmospheric Conditions

Kazufumi Kaneda, Takashi Okamoto, Eihachiro Nakamae, and Tomoyuki Nishita

ABSTRACT

A method for creating realistic images is proposed from the view point of displaying simulation results when designing a building in which various weather conditions are taken into account.

So far, in order to create realistic images for interior design, the concept of radiosity as ambient light including spectral distribution has been developed. The method can display not only the brightness but also the hue and saturation of color. In contrast, for designing a building sky light has been treated as ambient light, in which the brightness under various weather conditions could be calculated, but the influences on the hue and saturation of color were ignored.

The proposed method creates realistic images considering the brightness, hue and saturation under various atmospheric conditions by taking into account the spectral distribution of both direct sunlight and sky light. Views of buildings including the influences of the particles in the atmosphere, i.e. clouds, fog, and beams, are useful for design not only of new buildings but also of new city areas.

Key Words: Sky Light, Specular Reflectance, Atmospheric Scattering Model, Visual Environment, Building Design

1 INTRODUCTION

There are two approaches for rendering images: one is displaying realistic images for entertainment and art, and the other is displaying simulation results for environmental assessment and building design. We take the latter approach in this paper.

For designing and pre-evaluating a building, it is particularly desirable to display not only the figures of the completed building but also its images with the surroundings under various atmospheric conditions. A building has its own attributes such as color and reflection. However when it is lit by the sunlight under various atmospheric conditions, the hue of the building changes greatly, as well as its brightness and saturation, caused by various influences such as spectral distribution and intensity of light sources (direct sunlight and sky light in our applications) which are determined by the position of the sun and atmospheric conditions, and the relationship between the position of the building and the various objects obscuring it.

We propose here a method for displaying realistic images of 3-D objects, i.e. buildings, and particles in the atmosphere, i.e. cloud and haze, under various atmospheric conditions taking account of the spectral distribution of direct sunlight and sky light as an ambient light source.

Both direct light and ambient light should be taken into account in order to simulate lighting effect for environmental assessment, and so far the following methods have been developed.

For direct light, in the 1970s, a parallel light source was usually used. In the 1980s, methods for shading and shadowing 3-D objects lit by various artificial light sources such as a point light source [Nishita 85a], a linear light source [Nishita 85a], an area light source [Nishita 83], etc. were developed by the authors. In 1987, Klassen [Klassen 87] proposed a method for displaying the color of the sun and the hue of the sky taking into account both scattering and absorption of the sunlight due to air molecules and aerosols in the atmosphere. Inakage [Inakage 89] improved Klassen's method by approximating geometric optics for large particles such as raindrops, but the method is inadequate to generate realistic images for visual assessment because of not taking into account sky light and specular reflectance.

For ambient light, in the 1970s, the methods of adding either an uniform ambient light to the lighting model or a secondary light source coincident with the viewpoint was employed. In order to calculate exactly ambient light inside a room, Cohen et al. [Cohen 85] and the authors [Nishita 85b] proposed a method considering the inter-reflection of light, so called radiosity. In the former the phenomenon of color bleeding can be rendered, i.e., not only brightness but also hue and saturation of color are taken into account. Furthermore, Immel et al. [Immel 86] and Kajiya [Kajiya 86] developed a method considering specular reflectance, and Rushmeier et al. [Rushmeier 87] generalized the radiosity method for displaying beams of light due to particles in the atmosphere in a room. On the other hand, for ambient light in the open air the authors [Nishita 86] proposed a method for shading and shadowing taking into account of sky light. This method, however, only can display the brightness under various weather conditions, without the influences on the hue and saturation of color caused by spectral distribution of sky light.

Here a method for creating realistic images of outdoor 3-D objects such as buildings and streets considering specular reflection is proposed. In our proposed method, based on Klassen's model, the colors of the sun and sky, calculated by using the atmospheric scattering model and the spectral distribution of sunlight, are employed for direct sunlight and sky light. Ways to display not only shading and shadowing but also beam and fog effects caused by the direct sunlight and sky light with spectral distributions are described. The proposed method can create outdoor images taking account of hue, brightness, and saturation.

Further an improvement to Klassen's model concerning calculation of the color of the sun and sky is described in the next section. Rendering 3-D objects and clouds lit by direct sunlight and sky light are the topics of Section 3 and Section 4, respectively, and beam and fog effects are discussed in Section 5.

2 IMPROVEMENT OF THE ATMOSPHERIC SCATTERING MODEL

It is well known that sunlight is scattered or absorbed by the ozone layer, air molecules, and aerosols, as it passes through the atmosphere. Generally speaking, for visible wavelengths of light, absorption in the ozone layer is negligible compared with absorption by air molecules and aerosols. For particles small compared with the wavelength of the light, i.e. air molecules, Rayleigh scattering predominates. On the other hand, for large particles of a size larger than the wavelength of the light, i.e. aerosols, Mie scattering predominates.

In Klassen's atmospheric scattering model the distribution of Rayleigh particles is divided into two layers with uniform distributed particles in each layer. In fact, the density of air molecules decreases exponentially with altitude. Then, taking into account the density ratio of air molecules to the standard atmosphere (molecular density at sea level,) the light reflected due to Rayleigh scattering is calculated. The molecular density ratio ρ depends on the altitude h and is given by

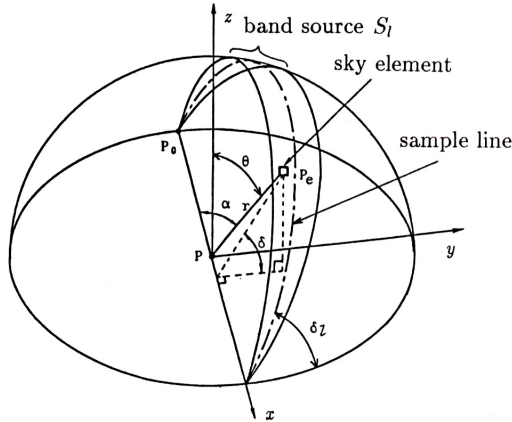$$\rho = \exp(-\frac{h}{H_0}), \tag{1}$$

Figure 1: Subdivision of the sky dome into band sources (P : calculation point)

where H_0 is a scale height ($H_0 = 7994 \, [\text{m}]$), which corresponds to the atmosphere thickness if the density were uniform.

For calculation of the sunlight scattered by aerosols, in Klassen's model the aerosols distribute in a flat layer. When the altitude of the sun is low, i.e. the case of dawn or sunset, the distance between the sunlight and the calculation point, passing through the atmosphere with aerosols, becomes infinite. To deal with this problem, the spherical-shell atmosphere model used for the air molecules mentioned above is used. From the view point of a macro-sized object like the earth, the density of aerosols decreases exponentially with altitude, like the density distribution of air molecules does, even though the rate of decrease is different from that of air molecules. The density can be calculated by setting the scale height, H_0, of Eq. 1 to 1.2 km [Sekine 87]. Displaying fog, in which the density has a different distribution from that mentioned above and is much higher, is described in Section 5.

3 RENDERING 3-D OBJECTS LIT BY SKY LIGHT

The method for rendering 3-D objects lit by sky light calculated by using the improved atmospheric scattering model taking account of its spectral distribution is described here.

The sky is taken as a hemisphere light source with a large radius (called the sky dome). The dome is subdivided into bands in the same way as those of reference [Nishita 86], and in each band the intensity of light varies in the band axis direction and is fixed at a constant value in the width direction (See Figure 1). In the case of the diffuse reflectance described in [Nishita 86], the band width is allowed to be fairly wide and is fixed because of the constant intensity of diffuse reflectance in every direction. On the other hand, it is well known that the intensity of the specular reflectance tends to the specified direction. Therefore, in this case a part of the sky dome may be enough for the calculation of specular reflectance even though the band width is narrow.

3.1 Specular Reflectance due to Sky Light

For calculation of specular reflectance due to sky light, the Cook-Torrance model [Cook 82] is employed, because of its suitability for rendering metallic objects and the fact that it takes into account the spectral distribution.
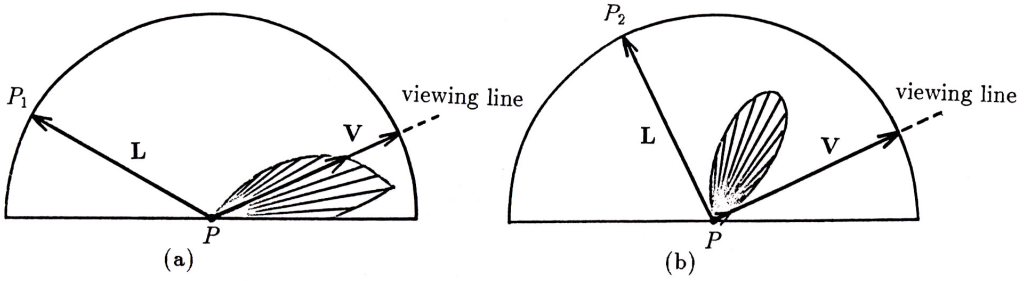
Figure 2: Specular reflectance due to the sky element

Let's assume that a sky element, a small area in a band source, is treated as a point light source, P_e, and the position of P_e is defined by the angle α from the x-axis to the sky element and the angle δ from the horizontal plane to the sky element (See Figure 1). By adding the effect of the specular reflectance to Eq. 1 in [Nishita 86], the intensity of the specular reflectance at P due to the sky element is given by the following equation:

$$dI = R_s(\alpha, \delta, \mathbf{V}) \cdot L(\alpha, \delta) \cdot \sin\alpha \cdot \sin\delta \cdot r^{-2} \cdot dA, \tag{2}$$

where $R_s(\alpha, \delta, \mathbf{V})$ is the coefficient of the specular reflectance, $\mathbf{V}$ is the unit vector from the calculation point P toward the viewpoint, $L(\alpha, \delta)$ is the intensity of the sky element, r is the distance PP_e, and dA is the area of the sky element and is given by

$$dA = (r \cdot d\alpha) \cdot (r \cdot d\delta \cdot \sin\alpha). \tag{3}$$

By integrating Eq. 2, the intensity of the specular reflectance due to the band source S_l is obtained as

$$I_l = \int_0^\pi \int_{\delta_l - \Delta_l}^{\delta_l + \Delta_l} R_s(\alpha, \delta, \mathbf{V}) \cdot L(\alpha, \delta) \cdot \sin\delta \cdot \sin^2\alpha \cdot d\delta \cdot d\alpha. \tag{4}$$

In such a narrow band as defined above, $\delta_l - \Delta_l \leq \delta < \delta_l + \Delta_l$ ($2\Delta_l$ is the angular width of a band source), both the intensity of the sky element and the coefficient of the specular reflectance can be held constant. Then $L(\alpha, \delta)$ and $R_s(\alpha, \delta, \mathbf{V})$ are expressed by $L(\alpha, \delta_l)$ and $R_s(\alpha, \delta_l, \mathbf{V})$, respectively. In this paper, the angle δ is sampled as $\cos(\delta_l - \Delta_l) - \cos(\delta_l + \Delta_l) = 1/N$ (constant). Thus, Eq. 4 becomes

$$I_l = \frac{1}{N} \cdot \int_0^\pi R_s(\alpha, \delta_l, \mathbf{V}) \cdot L(\alpha, \delta_l) \cdot \sin^2\alpha \cdot d\alpha. \tag{5}$$

Then, the intensity of the specular reflectance due to the sky dome is given by

$$I = \sum_{l=1}^N I_l, \tag{6}$$

where N is the number of the band sources.

3.2 Calculation of Specular Reflectance

It is almost impossible to obtain look-up tables like those for the intensity of the diffuse reflectance, because the coefficient of specular reflectance depends on the direction of the viewing line. Using the following property of specular reflectance, however, may save calculation time: if the direction of regular reflection of the sky element P_1 is almost coincident with the direction of viewing line as
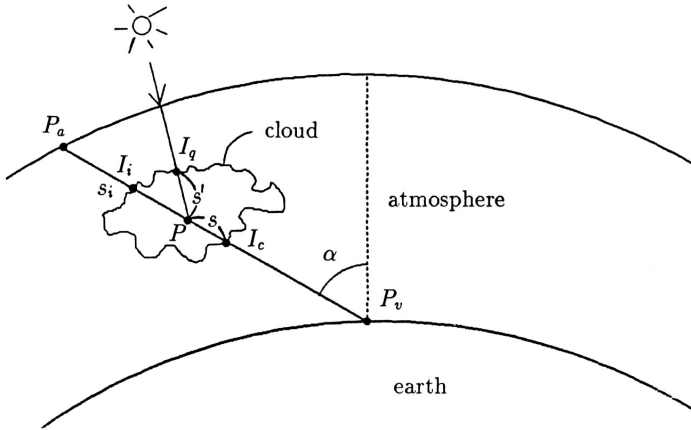
Figure 3: Determination of the integral region for specular reflectance

shown in Figure 2 (a), the intensity of the specular reflectance toward the viewing line is extremely large, and if not as shown in Figure 2 (b), much less intensity of specular reflectance due to the element, P_2, arrives at the viewpoint. These facts suggest that the intensity of specular reflectance due to the sky dome can be calculated without any compensation for preciseness by integrating a part of the sky dome in Eq. 6, that is, with an appropriate integral width and range.

If we define the function to determine the integral range for the sky element P_e as follows:

$$G(\alpha, \delta, \mathbf{V}) = L(\alpha, \delta) \cdot R_s(\alpha, \delta, \mathbf{V}) \cdot \sin \alpha, \tag{7}$$

and set a threshold value ε, then the integral range is limited in the regions where $G(\alpha, \delta, \mathbf{V})$ is greater than ε. The integral area cannot be determined a priori, because the function not only depends on the specular distribution of the lit object but also some objects casting their shadows on it affect the area. The integral starts from a location where the function has a large value and proceeds to a small value area, that is, from the sky element in the direction of the regular reflection to away from the sky element. The details of the integration is as follows (See Figure 3):

(1) Obtain the point, Q, where the direction of the regular reflection for the viewing line intersects with the sky dome. We assume that the point Q is located between two sample lines of the band sources S_l and S_{l+1}, where a sample line is defined by the center line of the band source. Then the tilt angle δ_l of the sample plane which is defined as the plane including the sample line of the band source, S_l, and x-axis is calculated.

(2) Search for the sky element P_l which is closest to the point Q along the sample line of the band source S_l, and calculate the angle α_{l1} between x-axis (PP_0) and PP_l. If $G(\alpha_{l1}, \delta_l, \mathbf{V}) \geq \varepsilon$, then integrate over the band source S_l as follows:

(2.1) Execute trapezoidal integration along the sample line from the sky element $P_l(\alpha_{l1}, \delta_l)$ toward one of the end of the line with a pitch $d\alpha$ corresponding to the width of a segment, until the condition, $G(\alpha_{l1}, \delta_l, \mathbf{V}) < \varepsilon$, is satisfied. When a segment of the sample line is obscured by some objects, the integral of that segment is skipped. The visible segments are obtained by calculating the intersections of the sample plane and those objects.

(2.2) Integrate the sample line from the sky element $P_l(\alpha_{l1}, \delta_l)$ toward the other end of the line in the same way as explained in (2.1).

Figure 4: Scattering due to clouds

(3) For an adjacent band source S_{l-1}, the process (2) is employed, when $G(\alpha_{l1}, \delta_l, \mathbf{V}) > \varepsilon$ at the border of S_l.

(4) Continue the above-mentioned process for the band sources S_{l-2}, S_{l-3} and so on. If at the P_i which is the closest sample segment to the point Q on the sample line of the band source S_i $(i = l - 1, l - 2, \cdots, 1)$ the condition, $G(\alpha_{i1}, \delta_i, \mathbf{V}) < \varepsilon$, is satisfied, then the integral is suspended.

(5) For the other side of the band sources, $S_{l+1}, S_{l+2}, \cdots, S_i, \cdots, S_N$, the processes from (2) to (4) are employed until the condition, $G(\alpha_{i1}, \delta_i, \mathbf{V}) < \varepsilon$, is satisfied.

4   CLOUDS

The size of particles in clouds is larger than that of air molecules or of aerosols mentioned before. Light scattered by large particles such as those in clouds is little influenced by wavelength. However, the spectral distribution of the sunlight onto clouds depends to a fair degree on the position of the sun. Therefore, the light passing through a cloud should be determined by the following three components: i) sky light attenuated by passing through the cloud, ii) light scattered and absorbed by cloud particles illuminated by direct sunlight, and iii) ambient light caused by multiple scattering due to atmospheric particles and cloud particles.

For i), the intensity of sky light, I_i, toward the viewpoint is obtained by using the before-mentioned atmospheric scattering model. For ii), the intensity of direct sunlight, I_q, is assumed to be constant everywhere on the face of a cloud because the cloud thickness is much smaller than that of the atmosphere. Therefore when the distance between the cloud center and the top of the atmosphere is Q, the intensity of direct sunlight on the cloud surface is given by

$$I_q = I_s(\lambda) \exp(-t(Q, \lambda)), \qquad (8)$$

where $I_s(\lambda)$ is the solar radiation at the top of the atmosphere, and $t(Q, \lambda)$ is the optical length of the distance Q for the wavelength λ. For iii), ambient light due to atmospheric particles is obtained by using the model mentioned before, and ambient light due to cloud particles is assumed to have uniform intensity for all directions.
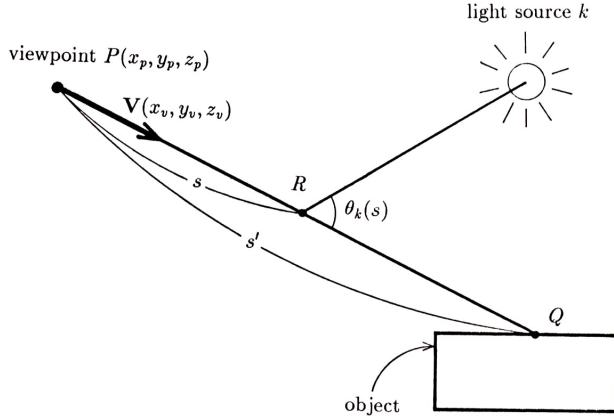
Figure 5: Calculation of the particle density

Finally, the intensity of light just after passing through the cloud, I_c, taking into account the three components mentioned above, is obtained by the following equation (See Figure 4):

$$I_c(\lambda) = I_i(\lambda) \cdot \exp(-t(s_i)) + \int_0^{s_i} (I_q(\lambda) \cdot F(\theta) + I_a) \cdot \exp(-t(s) - t(s')) \cdot \rho_c(s) \cdot ds, \qquad (9)$$

where I_a is the ambient light, and both the phase function F and the density of the cloud, ρ_c, are assumed to be uniform. The shape of the cloud is defined by mapping a thickness function (Fourier series composed of a polynomial of sine waves [Gardner 85]) onto an ellipse.

5   BEAM AND FOG EFFECTS

The space where light passes through atmosphere with vapor and particles brightens, and the intensity of the light weakens before arriving at the viewpoint, because the light is scattered or absorbed by these particles.

Displaying beam and fog effects caused by direct sunlight and sky light calculated by using the atmospheric scattering model is described here.

In Max's model [Max 86], the particles distribute in a flat layer; however, it is well known that the density of particles which cause beam or fog, density of vapor and aerosols, decreases in an exponential or similarway. If the distribution of particles is approximated as an exponential function, and a unit vector from the viewpoint P (x_p, y_p, z_p) to the point Q is expressed by $\mathbf{V}$ (x_v, y_v, z_v), then the particle density at a point R is given by the following equation (See Figure 5):

$$\rho(s) = \rho_0 \cdot \exp(-\frac{z(s)}{h_0}), \qquad (10)$$

where ρ_0 is the particle density at the altitude of zero meters, h_0 is a scale height for the particles, and $z(s) = z_p + z_v \cdot s$, where s is the distance between the points P and R. The attenuation coefficient, the scattering ratio of light during passing through a unit distance in the atmosphere, is proportional to the particle density and is given by

$$\tau(s) = \rho(s) \cdot \tau_0 \cdot (\frac{\lambda}{\lambda_0})^{-b}, \qquad (11)$$

where λ is the wavelength of incident light, λ_0 is a standard wavelength, τ_0 represents the scattering coefficient of the standard wavelength with unit particle density, and b is a coefficient decided by particle size of fog. Then, the optical length, $t(s)$, from the viewpoint P to the point R is obtained by

$$t(s) = \int_0^s \tau(s) \cdot ds. \tag{12}$$

If the distance between P and Q is s' and the intensity of the surface at Q is I_0, the intensity of the ray arriving at the viewpoint P is given by

$$I = I_0 \cdot \exp(-t(s')) + \sum_k \int_0^{s'} \tau(s) \cdot J_k(s) \cdot \exp(-t(s)) \cdot ds, \tag{13}$$

where $J_k(s)$ is the light function of the light source k at the viewpoint P and is given by

$$J_k(s) = I_k(s) \cdot \exp(-t'_k(s)) \cdot F(\theta_k(s)), \tag{14}$$

where $I_k(s)$ represents the intensity of the ray arriving at the point R under the condition of no particles and is calculated by direct sunlight and sky light which are obtained by the atmospheric scattering model, $t'_k(s)$ is an optical distance between the light source k and the point R, and $F(\theta_k(s))$ is a phase function.

For displaying beams taking into account obstacles, the integration is performed only for visible sections of light on the viewing line, where the section is obtained by using shadow volumes [Nishita 87]. Integration in the cases of direct sunlight and sky light is described below.

5.1   Direct Sunlight

$F(\theta_k(s))$ in Eq. 14 has a constant value, because $\theta_k(s)$ is constant as the direct sunlight is a parallel light source. Then, Eq. 13 is able to be calculated analytically (See Appendix).

5.2   Sky Light

Beams often appear when direct sunlight with high intensity is passing through particles in the atmosphere. On the other hand, when the component of sky light is larger than that of direct sunlight, i.e. in a fog or a mist, the whole atmosphere illuminated by the sky light is brightened. In the latter case, Eq. 13 must be calculated by using numerical integration because the analytical integration used for a parallel light source (direct sunlight) cannot be employed. For simplifying the calculation, we assume the conditions of a uniform phase function and no shadow effects of obstacles in this case.

The intensity of sky light, $J_k(s)$, arriving at the point P_i (See Figure 6) is obtained by integrating the sky elements along all band sources which the sky dome is divided into, that is,

$$J_k(s_i) = \sum_{l=1}^{N} W_l \cdot \int_0^\pi L(\alpha, \delta) \cdot \sin \alpha \cdot \exp(-t'(s_i)) \cdot d\alpha, \tag{15}$$

where N is the number of the band sources, W_l is the angular width of the band source l, $L(\alpha, \delta)$ is intensity of sky light, and $t'(s_i)$ is a optical distance between the point P_i and each sky element.

By introducing the two assumptions described above, $J_k(s_i)$ can be expressed by only the function of the altitude of P_i; in other words, the relationship with the x and y coordinates of the point P_i
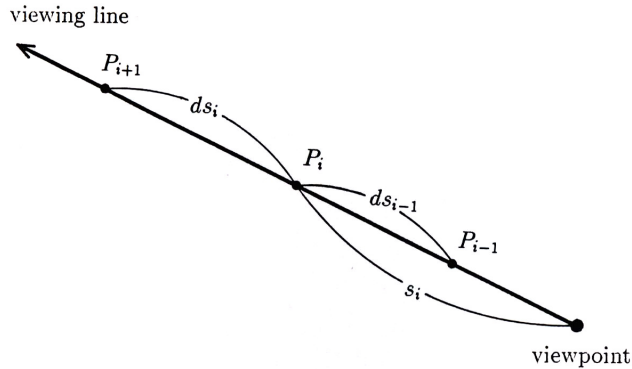
Figure 6: Numerical integral for displaying fog effect caused by sky light

and the directions of viewing line and ray may be neglected. Therefore, look-up tables of $J_k(s_i)$ at every altitude can be created in advance.

Trapezoidal integration is employed for integrating the intensity of the scattered light along the viewing line. That is, the integral starts from the viewpoint with a pitch, ds_i, which is determined by using the following equation (See Figure 6):

$$ds_i = \max(ds_{min}, \min(ds_{max}, \frac{ds_0}{\tau(s_i) \cdot J_k(s_i) \cdot \exp(-t(s_i))})), \tag{16}$$

where ds_{min} and ds_{max} are the minimum and maximum pitches, respectively, and ds_0 is a standard pitch. The integral is continued until the condition, $\tau(s_i) \cdot J_k(s_i) \cdot \exp(-t(s_i)) < \varepsilon$, is satisfied.

6 EXAMPLES

Figure 7 shows an application to building design. The walls of the building in Figures (a) through (c) are made of white tiles (which have mainly diffused reflectance), and the material in Figures (d) through (f) is aluminum (which has almost only specular reflectance). Figures (a) and (d) are the case of early morning (solar altitude is 8 degrees), Figures (b) and (e) are also in the morning (20 degrees), and Figures (c) and (f) are at sunset (3 degrees). These figures demonstrate not only the variation in the hue and brightness of the building but also that of the sky color. Figures (a) through (c) show the variation of the hue of the building due to sun position. Human eyes usually don't perceive such a large differences of the hue on the walls, even though actual color varies as shown in these figures. Because human visual perception takes into account expectations of color and color difference of various objects in the environment rather than their absolute spectral distribution, people do not ordinarily notice this type of color shift.

Figures (b) and (e) show that the color of the highlight on the building is mainly influenced by specular reflectance of the direct sunlight, and Figures (d) through (f) show that except for the highlight region the hue of the building varies according to the sky light. In Figures (a) through (c), the influence of the hue of sky light comes out on the walls whose surface is nearly parallel to the viewing line, because the more parallel the reflection plane is to the viewing line, the greater the effects on the specular reflectance component.

It is assumed that in Figure 8, the position of the sun was behind the building. In this figure, where the sun is in front of the viewpoint, the edges of the clouds are brighter than their central area because of their thickness. When the sun is behind the viewpoint, on the other hand, as in Figure 7, the side of the clouds lit by direct sunlight is brighter than the other side.
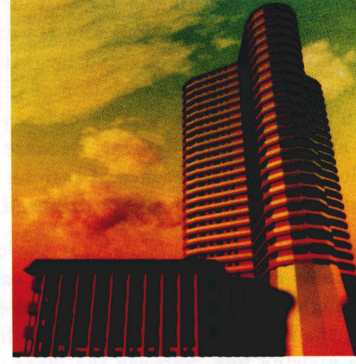
sorlar altitude \ material	tile	aluminum
early morning 8°	(a)	(d)
morning 20°	(b)	(e)
sunset 3°	(c)	(f)

Figure 7: Examples of changing color of the building according to the solar altitude and the material of the walls

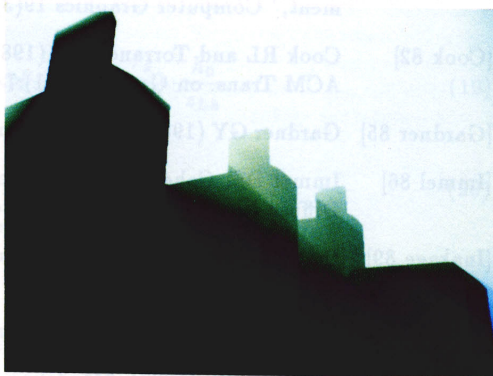**Figure 8: Example of the counter-light**
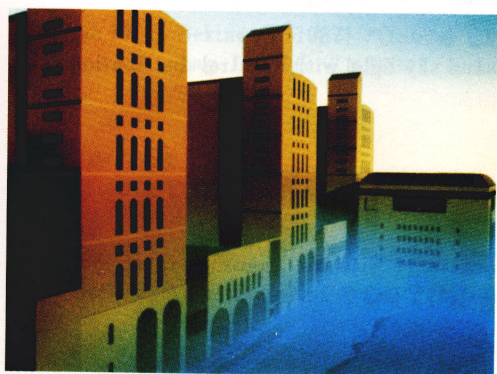
(a)	(b)
(c)	(d)

Figure 9: Examples of beam and fog effects

Figure 9 demonstrates how fog reacts to direct sunlight as well as sky light and shows the variation in the appearance of the buildings. In Figure (a), the parameters ρ_0 and h_0 (in Eq. 10) are set to 0.59 and 10.0, respectively, so the higher the altitude, the lower the density. On the contrary, in Figure (b), the parameters ρ_0 and h_0 are set to 0.037 and -15.0, respectively. Figures (c) and (d) display the silhouette and beam effects. In the former, ρ_0, h_0, and the sun altitude are 0.16, 80.0, and 40 degrees, and in the latter, 0.088, 80.0, and 35 degrees. By using IRIS-4D/70GT, it took about 17 and 20 hours to calculate Figures 8 and 9 (a), respectively.

7 CONCLUSIONS

A method for displaying realistic outdoor images taking into account the spectral distribution of both direct sunlight and sky light is proposed from the view point of displaying the simulation results for designing buildings and performing assessments of their environmental impacts.

The proposal described in this paper has the following advantages:

1. The hue of the sky, clouds, and buildings vary according to both the position of the sun and atmospheric conditions.

2. Buildings lit by both direct sunlight and sky light can be displayed taking into account specular reflectance.

3. Fog and beam effects caused by direct sunlight and sky light with spectral distribution can be displayed.

Acknowledgment

REFERENCES

[Cohen 85]   Cohen MF and Greenberg DP (1985) "A Radiosity Solution for Complex Environment," Computer Graphics 19(3):31-40

[Cook 82]   Cook RL and Torrance KE (1982) "A Reflectance Model for Computer Graphics," ACM Trans. on Graphics 1(1):7-24

[Gardner 85]   Gardner GY (1985) "Visual Simulation of Cloud," Computer Graphics 19(3):297-303

[Immel 86]   Immel DS, Cohen MF, and Greenberg DP (1986) "A Radiosity Method for Non-Diffuse Environments," Computer Graphics 20(4):133-142

[Inakage 89]   Inakage M (1989) "An Illumination Model for Atmospheric Environment," Proc. CGI'89 :533-548

[Kajiya 86]   Kajiya JT (1986) "The Rendering Equation," Computer Graphics 20(4):143-150

[Klassen 87]   Klassen RV (1987) "Modeling the Effect of the Atmosphere on Light," ACM Trans. on Graphics 6(3):215-237

[Max 86]   Max NL (1986) "Atmospheric Illumination and Shadows," Computer Graphics 20(4):117-124

[Nishita 83]   Nishita T and Nakamae E (1983) "Half-Tone Representation of 3-D Objects Illuminated by Area Sources or Polyhedron Sources," IEEE COMPSAC :237-242

[Nishita 85a]   Nishita T, Okamura I, and Nakamae E (1985) "Shading Models for Point and Linear Sources," ACM Trans. on Graphics 4(2):124-146

[Nishita 85b]   Nishita T and Nakamae E (1985) "Continuous Tone Representation of Three-Dimensional Objects Taking Account of Shadows and Interreflection," Computer Graphics 19(3):23-30

[Nishita 86]   Nishita T and Nakamae E (1986) "Continuous Tone Representation of Three-Dimensional Objects Illuminated by Sky Light," Computer Graphics 20(4):125-132

[Nishita 87]   Nishita T, Miyawaki Y, and Nakamae E (1987) "A Shading Model for Atmospheric Scattering Considering Distribution of Light Sources," Computer Graphics 21(4):303-310

[Rushmeier 87]   Rushmeier HE, Torrance KE (1987) "The Zonal Method for Calculating Light Intensities in the Presence of a Participating Medium," Computer Graphics 21(4):293-302

[Sekine 87]   Sekine S (1987) "Optical Characteristics of Turbid Atmosphere," J. Illum. Engng. Int. Jpn. 71(6):333 (in Japanese)

APPENDIX
INTENSITY OF PARALLEL LIGHT SCATTERED BY FOG

We assume that fog distributes in a flat layer because fog usually distributes in a local area.

The illuminance at the point R and $F(\theta_k(s))$ without fog is given by

$$I_k(s) = I_k, \tag{17}$$

$$F(\theta_k(s)) = F_k, \tag{18}$$

where both I_k and F_k have a constant value because of a parallel light (See Figure 10). By integrating the attenuation coefficient between the point R and the light source (the distance is infinite), its optical distance, $t'(s)$, is given by

$$t'(s) = \rho_0 \cdot \tau_0 \cdot \left(\frac{\lambda}{\lambda_0}\right)^{-b} \cdot \exp\left(-\frac{z_p + z_v \cdot s}{h_0}\right) \cdot \frac{h_0}{z_{Lk}}. \tag{19}$$

Then, the light function, $J_k(s)$, is given by

$$J_k(s) = I_k \cdot F_k \cdot \exp(-t'(s)). \tag{20}$$

Intensity of light scattered by fog between s_1 and s_2 is given by

$$I = \int_{s_1}^{s_2} \tau(s) \cdot J_k(s) \cdot \exp(-t(s)) \cdot ds. \tag{21}$$

To simplify this equation, the following substitution is introduced:

$$\alpha = \rho_0 \cdot \tau_0 \cdot \left(\frac{\lambda}{\lambda_0}\right)^{-b} \cdot \exp\left(-\frac{z_p}{h_0}\right). \tag{22}$$

Then, Eq. 21 is solved by

(1) for $z_v = 0$,

$$I = I_k \cdot F_k \cdot \int_{s_1}^{s_2} \exp(-\alpha \cdot \frac{h_0}{z_{Lk}}) \cdot \alpha \cdot \exp(-\alpha \cdot s) \cdot ds$$

$$= I_k \cdot F_k \cdot \exp(-\alpha \cdot \frac{h_0}{z_{Lk}}) \cdot [\exp(-\alpha \cdot s)]_{s_2}^{s_1}. \tag{23}$$

(2) for $z_v \neq 0$,

$$I = I_k \cdot F_k \cdot \int_{s_1}^{s_2} \alpha \cdot \exp(-\frac{z_v}{h_0} \cdot s) \cdot \exp(-\alpha \cdot \frac{h_0}{z_v}) \cdot \exp(\alpha \cdot h_0 \cdot (\frac{1}{z_v} - \frac{1}{z_{Lk}}) \cdot \exp(-\frac{z_v}{h_0} \cdot s)) \cdot ds. \tag{24}$$

Eq. 24 is solved by the following:

(2.1) for $z_v = z_{Lk}$,

$$I = I_k \cdot F_k \cdot \int_{s_1}^{s_2} \alpha \cdot \exp(-\alpha \cdot \frac{h_0}{z_v}) \cdot \exp(-\frac{z_v}{h_0} \cdot s) \cdot ds$$

$$= I_k \cdot F_k \cdot \alpha \cdot \exp(-\alpha \cdot \frac{h_0}{z_v}) \cdot \frac{h_0}{z_v} \cdot [\exp(-\frac{z_v}{h_0} \cdot s)]_{s_2}^{s_1}. \tag{25}$$

(2.2) for $z_v \neq z_{Lk}$,

We use the following integration by substitution:

$$u = f(s) = \exp(-\frac{z_v}{h_0} \cdot s). \tag{26}$$

Therefore,

$$\frac{du}{ds} = \frac{d}{ds} f(s) = -\frac{z_v}{h_0} \cdot \exp(-\frac{z_v}{h_0} \cdot s). \tag{27}$$

Then, Eq. 24 can be expressed by the following:

$$I = I_k \cdot F_k \cdot \int_{f(s_1)}^{f(s_2)} \alpha \cdot \exp(-\frac{z_v}{h_0} \cdot s) \cdot \exp(-\alpha \cdot \frac{h_0}{z_v}) \cdot \frac{1}{\frac{du}{ds}}$$

$$\cdot \exp(\alpha \cdot h_0 \cdot (\frac{1}{z_v} - \frac{1}{z_{Lk}}) \cdot u) \cdot du$$

$$= I_k \cdot F_k \cdot \frac{\exp(-\alpha \cdot \frac{h_0}{z_v})}{1 - \frac{z_v}{z_{Lk}}} \cdot [\exp(\alpha \cdot h_0 \cdot (\frac{1}{z_v} - \frac{1}{z_{Lk}}) \cdot u)]_{\exp(-\frac{z_v}{h_0} \cdot s_2)}^{\exp(-\frac{z_v}{h_0} \cdot s_1)}. \tag{28}$$
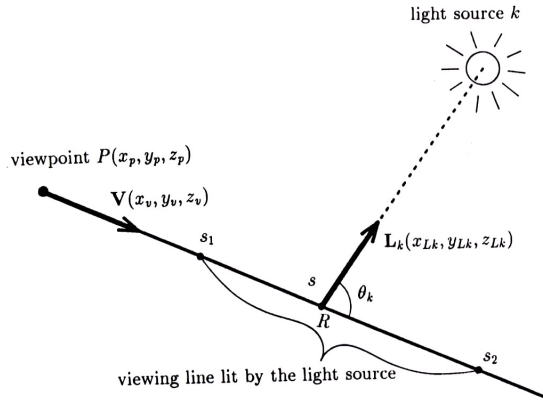

Figure 10: Analytical integral for displaying fog effect caused by direct sunlight

Kazufumi Kaneda is a research associate in Faculty of Engineering at Hiroshima University. He worked at the Chugoku Electric Power Company Ltd., Japan from 1984 to 1986. He joined Hiroshima University in 1986. His research interests include computer graphics and image processing.

Kaneda received the BE and ME in 1982 and 1984, respectively, from Hiroshima University. He is a member of IEE of Japan, IPS of Japan and IEICE of Japan.

Address: Faculty of Engineering, Hiroshima University, Saijo-cho, Higashi-hiroshima, 724 Japan.

E-mail: kin@eml.hiroshima-u.ac.jp
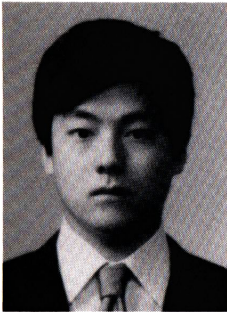
Takashi Okamoto is a graduate student in system engineering at Hiroshima University. His research interests include computer graphics and its application.

Okamoto received the BE degrees in electronics engineering in 1988 from Hiroshima University. He is a member of IPS of Japan.

Address: Faculty of Engineering, Hiroshima University, Saijo-cho, Higashi-hiroshima, 724 Japan.

Eihachiro Nakamae is a professor at Hiroshima University where he was appointed as research associate in 1956 and a professor in 1968. He was an associate researcher at Clarkson College of Technology, Potsdam, N. Y., from 1973 to 1974. His research interests include computer graphics and electric machinery.

Nakamae received the BE, ME, and DE degrees in 1954, 1956, and 1967 from Waseda University. He is a member of IEEE, IEE of Japan, IPS of Japan and IEICE of Japan.

Address: Faculty of Engineering, Hiroshima University, Saijo-cho, Higashi-hiroshima, 724 Japan.

E-mail: naka@eml.hiroshima-u.ac.jp

Tomoyuki Nishita is an associate professor in the department of Electronic and Electrical Engineering at Fukuyama University, Japan. He was on the research staff at Mazda from 1973 to 1979 and worked on design and development of computer-controlled vehicle system. He joined Fukuyama University in 1979. He was an associate researcher in the Engineering Computer Graphics Laboratory at Brigham Young University from 1988 to the end of March, 1989. His research interests involve computer graphics including lighting model, hidden-surface removal, and antialiasing.

Nishita received his BE, ME and Ph. D in Engineering in 1971, 1973, and 1985, respectively, from Hiroshima University. He is a member of ACM, IPS of Japan and IEE of Japan.

Address: Faculty of Engineering, Fukuyama University, Sanzo, Higashimura-cho, Fukuyama, 729-02 Japan.